Performance Improvements of Shack-Hartmann Sensors with Keystone Design Lenslet Arrays

M. E. Kasper[a,c], S. Hippler[a], S. Rabien[b]

[a]Max-Planck-Institut für Astronomie, Heidelberg, Germany
[b]Max-Planck-Institut für Extraterrestrische Physik, Garching, Germany
[c]European Southern Observatory, Garching, Germany

ABSTRACT

Shack-Hartmann based wavefront sensors, used to compensate atmospheric turbulence, appear to be less sensitive than curvature based wavefront sensors by more than a magnitude. Besides their read noise free APD detectors and different measurement principle, the sensitivity of curvature sensors may benefit from the keystone shaped lenslet geometry which optimally balances aperture coverage and illumination of individual subapertures. This paper describes the implementation of a keystone shaped lenslet array for the ALFA Shack-Hartmann based AO system. We compare the novel design with hexagonal shaped lenslets under different operating conditions such as selected modal basis set and number of compensated modes theoretically and in practice.

Keywords: Adaptive Optics, Wavefront Sensing, Shack-Hartmann Sensor, Keystone Lenslet Design

1. INTRODUCTION

Current operational Adaptive Optics (AO) systems use either Shack-Hartmann (SHS) or Curvature (CWS) wavefront sensors to measure aberrations introduced by turbulent refractive index variations in the atmosphere. Simulations predict a slightly superior low light level performance for CWS (Rigaut, Ellerbroek, and Northcott, 1997). This can be explained by the known advantages of the CWS, such as the robust first moment (sum) intensity measurement, read-noise free Avalache Photo Diode detectors, extra-focal distance as a tuning parameter, and an almost diagonal interaction matrix with bimorph deformable mirrors. Experience even shows evidence for a larger low light level gain of the CWS than the about one magnitude predicted by the simulations. The Keck AO system (SHS) for example has a limiting magnitude of about 14 while HOKUPA'A (CWS) can perform a low order wavefront correction on stars which are about two magnitudes fainter (Wizinowich et al., 2001). This comparison is especially meaningful since both AO systems operate at the same site.

In addition to the advantages mentioned above, all CWS use a keystone lenslet design, which is perfectly adapted to the annular pupil geometry of most astronomical telescopes. This design covers the telescope pupil with subapertures having the shape of annular segments as shown in the left drawing of Figure 1. If the subapertures in the different annuli are further designed such that they have similar sizes, they are equally illuminated, and the measurement noise is uniform. So far, SHS used lenslet arrays with rectangular or hexagonal subapertures, having the disadvantage that either the pupil is not fully covered or some subapertures are poorly illuminated producing noisier measurements.

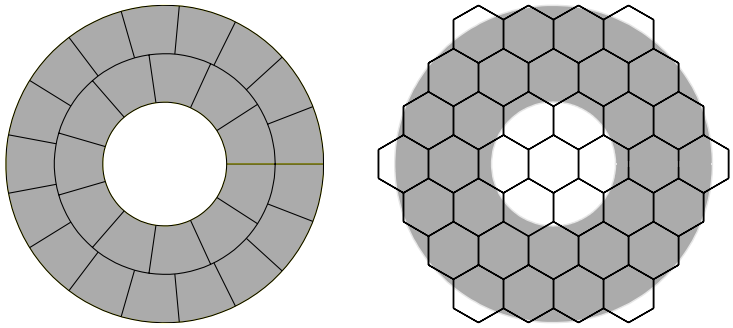

Figure 1. *Left*: Keystone lenslet geometry, 28 subapertures. *Right*: Hexagonal lenslet geometry, 30 subapertures.

This paper describes the keystone lenslet array implemented in the ALFA SHS AO system (Kasper et al., 2000). It also presents an analysis of wavefront reconstruction with keystone and hexagonal lenslet arrays and a comparison of the two methods at the telescope in closed loop.

2. KEYSTONE LENSLET ARRAY

The keystone lenslets were designed such that their height equals the length of the center arc as illustrated by the two dashed lines in Figure 2. The lens vertex is put at the intersection between them. The ALFA keystone array, displayed in Figure 1 on the left and hereafter labeled KS28, covers the telescope aperture with 28 lenslets. The telescope pupil, re-imaged on the lenslet array, has a diameter of 5 mm. Hence, the resulting lateral dimension of the individual lenslets is about 750 µm. Each lenslet covers an area of 0.29 m^2 in the telescope aperture. With a focal length of 45 mm, a maximum sag of about 3.5 µm at the subapertur edges results for a conventional lens of refractive index 1.5. Such an array was purchased from Adaptive Optics Associates, Cambridge, USA.

In addition, a similar lenslet array produced by a different technology called *mask-structured ion exchange* (MSI, see Bähr & Brenner, 2001) was tested. MSI creates lenslets by locally altering the refractive index in a planar glass substrate without modifying its surface. Figure 3 shows the spot pattern produced by this array. The central and outer parts of the array, which are not covered by lenses, are transparent and create stray and background light for our test setup. The individual spots have a diameter of about 49 µm, which is close to the diffraction limit of 42 µm at the measurement wavelength of 700 nm. The spot positions correspond to the lenslet vertexes within a few microns. This technique is capable of producing lenslets with numerical apertures as large as 0.1 – 0.2, and phase sags up to 50 waves at 632 nm (Bähr & Brenner, 2001).

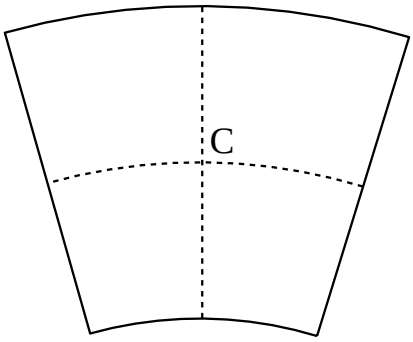

Figure 2. Keystone design lenslet.

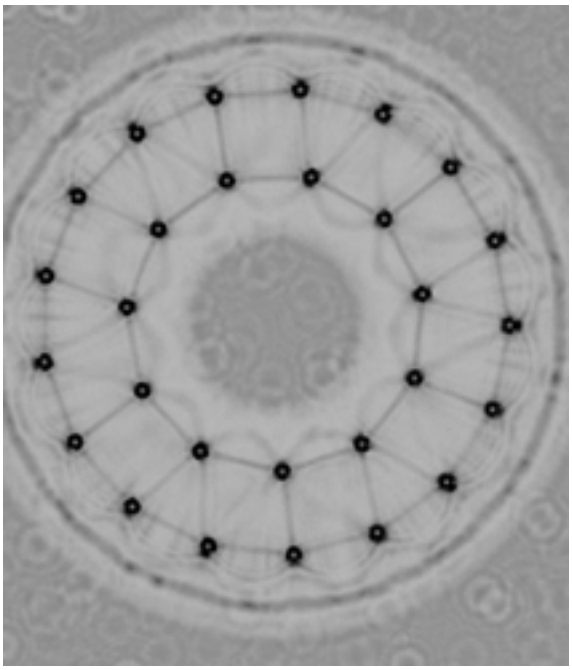

Figure 3. Logarithmic plot of the spot pattern produced by the MSI lenslet array.

3. KEYSTONE VS. HEXAGONAL DESIGN

The KS28 array described in the previous section and shown in Figure 1 is now compared to the likewise shown hexagonal array, hereafter called the HX30 array. The HX30 array effectively covers the 5 mm diameter pupil with 30 subapertures, the 7 innermost lenses being obscured by the secondary telescope mirror. The focal length of the lenslets is 45 mm, and single hexagons have side lengths of 450 µm. In the telescope aperture, this translates into a photon collecting area of about 0.26 m^2 for each subaperture.

3.1 Analysis of modal wavefront reconstruction

The modal control approach approximates the wavefront phase $\phi(x,y,t)$ by a superposition of a collection of n control modes $M_i(x,y)$, i.e. wavefront shapes, on the pupil:

$$\phi(x,y,t) \approx \sum_{i=1}^{n} a_i(t) M_i(x,y). \tag{1}$$

The modal coefficients a_i give the contribution of the corresponding mode to the wavefront. In AO dealing with atmospheric aberrations, equality of the two terms in Eq. 1 can only be reached for $n \to \infty$.

The measurement process in an SHS can be described by the following linear relationship:

$$\mathbf{g} = \mathbf{D}\mathbf{a} + \mathbf{D}_{\perp}\mathbf{a}_{\perp} + \mathbf{n}. \tag{2}$$

The columns of the interaction matrix **D** contain the gradients originating from the control modes. **D** can be calculated using a model of the wavefront sensor, or it can be measured during a calibration procedure. The measurement **g** is further affected by gradients from modes which complement the control modes to infinite dimension as described by their interaction matrix $\mathbf{D}_{\perp}$ weighted by the coefficients $\mathbf{a}_{\perp}$. This term is generally referred to as *modal aliasing*. Since atmospheric turbulence excites an infinite number of modes with varying amplitudes (Noll, 1976 or Wang&Markey, 1981), aliasing always exists and noiseless wavefront reconstruction is impossible. Finally, the measurement is corrupted by a noise-term **n** representing e.g. photon-, readout-, or quantization noise in the detector.

To reconstruct the wavefront, the modal coefficients have to be estimated from the measured gradients (wavefront slopes). Given a reconstruction matrix **R**, the estimate for the control mode coefficients can be written as

$$\hat{\mathbf{a}} = \mathbf{R}\mathbf{g} = \mathbf{R}\mathbf{D}\mathbf{a} + \mathbf{R}\mathbf{D}_{\perp}\mathbf{a}_{\perp} + \mathbf{R}\mathbf{n}. \tag{3}$$

Using the standard least-squares estimate (**R** is the pseudo-inverse of **D, RD** = **Id**), and assuming uncorrelated noise, the reconstruction error variance matrix of the control modes can be written as (Dai, 1996)

$$\left\langle (\mathbf{a}-\hat{\mathbf{a}})(\mathbf{a}-\hat{\mathbf{a}})^t \right\rangle = \mathbf{C}\left\langle \mathbf{a}_{\perp}\mathbf{a}_{\perp}^t \right\rangle \mathbf{C}^t + \mathbf{R}\left\langle \mathbf{n}\mathbf{n}^t \right\rangle \mathbf{R}^t, \tag{4}$$

where $\mathbf{C} := \mathbf{R}\,\mathbf{D}_{\perp}$, and <…> denote the ensemble average.

For an orthonormal set of modes such as Zernike polynomials or Karhunen-Loève (KL) functions, the total reconstruction error $\sigma_{t,n}^2$ is then given by summing up the reconstruction errors of the n control modes and the contribution of the high order modes which have not been estimated (usually called *fitting error*):

$$\sigma_{t,n}^2 = Tr\left(\left\langle (\mathbf{a}-\hat{\mathbf{a}})(\mathbf{a}-\hat{\mathbf{a}})^t \right\rangle\right) + \sum_{j=n+1}^{\infty} \left\langle a_j^2 \right\rangle. \tag{5}$$

Increasing n reduces the fitting error, but may increase the reconstruction error because non-orthogonal measurement vectors lead to ill-conditioned interaction matrices and hence noise amplification (Kasper et al., 2000). This phenomenon is known as *modal cross-talk* and was first analyzed by Hermann (1981).

Model calculations

A computer model of KS28 and HX30 was used to calculate the interaction matrices for a sufficiently large number of KL and Zernike modes. With the modal decomposition of atmospheric turbulence given by Noll (1976) for Zernike polynomials or by Wang & Markey (1982) for KL functions, $\sigma_{t,n}^2$ for different noise levels can be calculated as a function of n by Eq. 5.

Figure 4 shows the result of such a calculation. The general behavior for a least-squares (LS) reconstruction is a decrease of $\sigma_{t,n}^2$ with n until noise amplification dominates over the reduced fitting error. The optimum n corresponds roughly to the number of subapertures, i.e. half the number of measurements (X and Y gradients). Noise amplification does not occur for the Maximum A Posteriori (MAP) reconstruction algorithm also shown but not discussed here. The curve labeled as 'Optimum' represents the unrealistic case of a perfect reconstruction of the n control modes, i.e. with fitting error only. Table 1 lists the minimum least-squares reconstruction error variances obtained from Figure 4 as well as the corresponding n_{opt} in parentheses.

Both arrays perform better with the KL than with the Zernike basis set. Herby, the better fit to a turbulent wavefront with a certain number of KL modes plays only a minor role. More important is the reduced cross-talk of the KL modes with re-

spect to the Zernikes. This behavior was also observed when investigating other lenslet geometries such as a 18 subaperture haxagonal design.

If measurement noise is negligible (very bright guide star), the KS28 and the HX30 perform equally well with a KL basis set. The poor KS28 performance for Zernike polynomials is due to a strong cross-talk between defocus, and 2nd and 3rd order spherical aberrations (modes 10 and 21). For a SNR[1] of 5 (faint guide star), the KS28 is superior to the HX30 for both basis sets. The improved performance is due to the uniform noise achieved with the keystone array. For the hexagonal design poorly illuminated subapertures produce noisy gradients that may corrupt wavefront reconstruction. The problem of non-uniform noise could be overcome by use of an advanced estimator which considers measurement noise, such as the weighted least-squares estimator. With keystone arrays, a simple least-squares estimate already achieves satisfactory results.

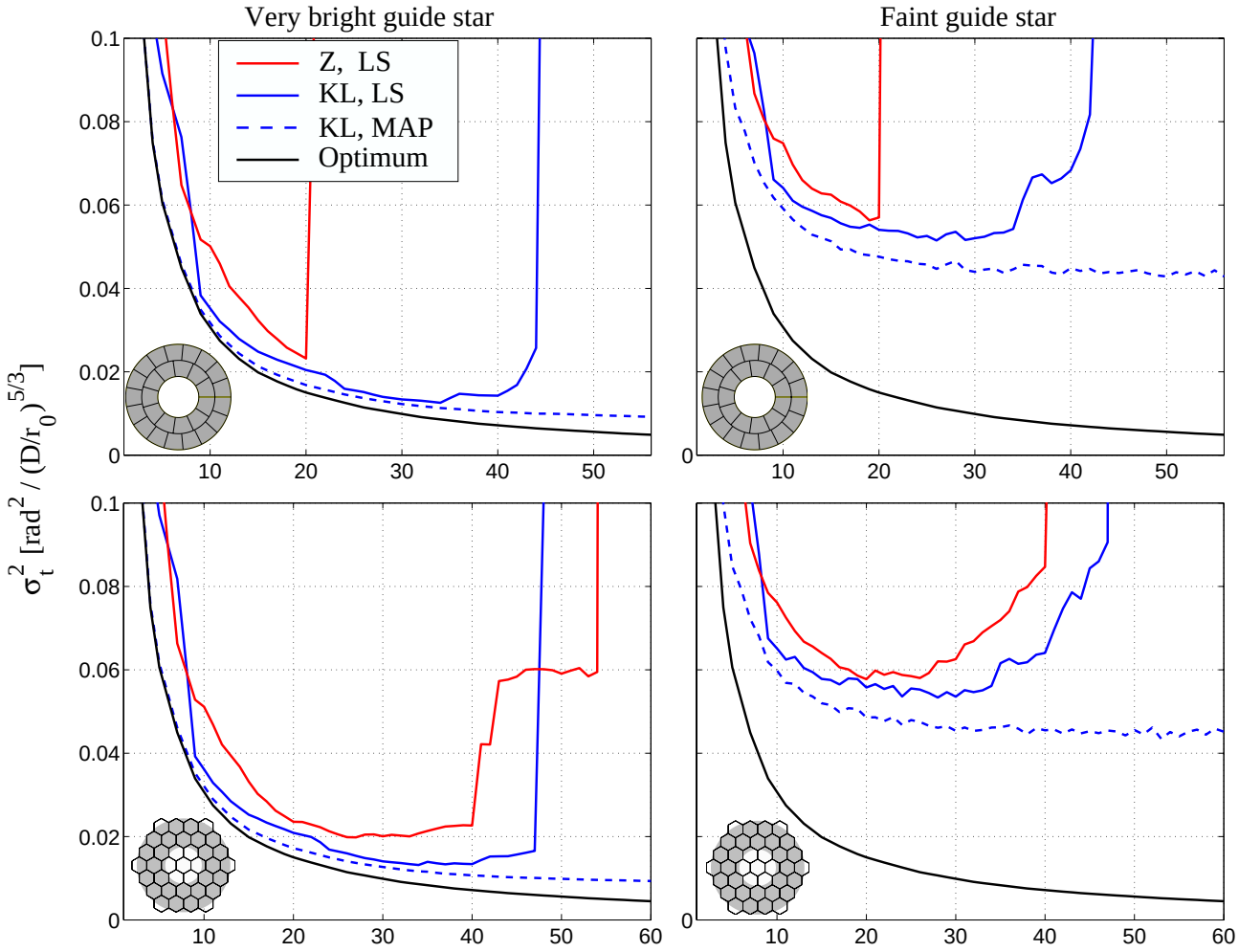

Figure 4. Total reconstruction error versus the number of reconstructed modes for the KS28 and HX30 lenslet arrays. The left figures resemble the case of an infinitely bright guide star (aliasing noise only), the right figures resemble the faint guide star case (SNR = 5) where measurement noise dominates.

Table 1. Minimum least-squares reconstruction error variance in [rad^2] for an optimum number of reconstructed modes derived from Figure 4. The values are normalized, i.e. they should be multiplied by $(D/r_0)^{5/3}$.

	KS28		HX30	
	KL	Z	KL	Z
$\sigma_{t,min}^2$ (n_{opt}), high SNR	0.013 (34)	0.023 (20)	0.013 (34)	0.02 (27)
$\sigma_{t,min}^2$ (n_{opt}), low SNR	0.049 (29)	0.056 (20)	0.053 (28)	0.058 (20)

[1] The SNR is defined as the ratio between the average aberration signal $\mathbf{Da} + \mathbf{D}_\perp \mathbf{a}_\perp$ and the noise-term $\mathbf{n}$.

3.1 Comparison to experiment

Setup

In order to compare the effect of the lenslet array geometry on image quality, we used the KS28 or the HX30 array to close the AO loop with ALFA on the $m_V = 7.5$ natural guide star (NGS) SAO 54431. The modal wavefront reconstruction was set to estimate 34 KL like modes including tip and tilt using the least squares method. The number of 34 modes appeared to be optimum for both arrays under bright guide star conditions as indicated by the simulations. During the experiment, ALFA was operated at a framerate of 200 Hz.

Sets of 10 K-band exposures of 2 seconds each were taken with the Omega-Cass (Lenzen et al., 1998) near-infrared camera for both lenslet arrays, and Strehl ratios were computed for all individual images. In order to eliminate effects that could be introduced by variable observing conditions, 24 of these sets were taken in a completely randomized order. The 24 image sets divide into 12 sets for each lenslet configuration, i.e. 120 individual images. Additionally, one set with tip-tilt only correction was recorded intermittently to estimate the observing conditions. The FWHM of the tip-tilt corrected K-band PSF was 0.5", indicating a V-band seeing of about 0.8".

To simulate a faint guide star, an ND2 filter was put in front of the wavefront sensor, dimming the star by 5 magnitudes down to $m_V = 12.5$. The number of corrected modes was set to 28 as suggested by the simulations, and the framerate was lowered to 50 Hz to reduce the impact of readout noise. Again, 24 image sets of ten two seconds exposures were recorded, switching randomly between the arrays.

Results

The 120 Strehl ratio measurements for each configuration are plotted in Figure 5. The individual images show K-band Strehl ratios of above 70% in the best cases. Apparently, the improvement with the KS28 is less obvious in the bright guide star case shown on the left. Both distributions are fairly similar besides the few very high Strehl ratios achieved with the KS28. This result was predicted by the simulations and was expected, because in the bright guide star case, the AO performance is determined by the degrees of freedom. In the faint guide star case, where noise is the limiting factor, the KS28 clearly shows an improved image quality with a mean Strehl ratio of 29.1% compared to the 24.2% achieved with the HX30.

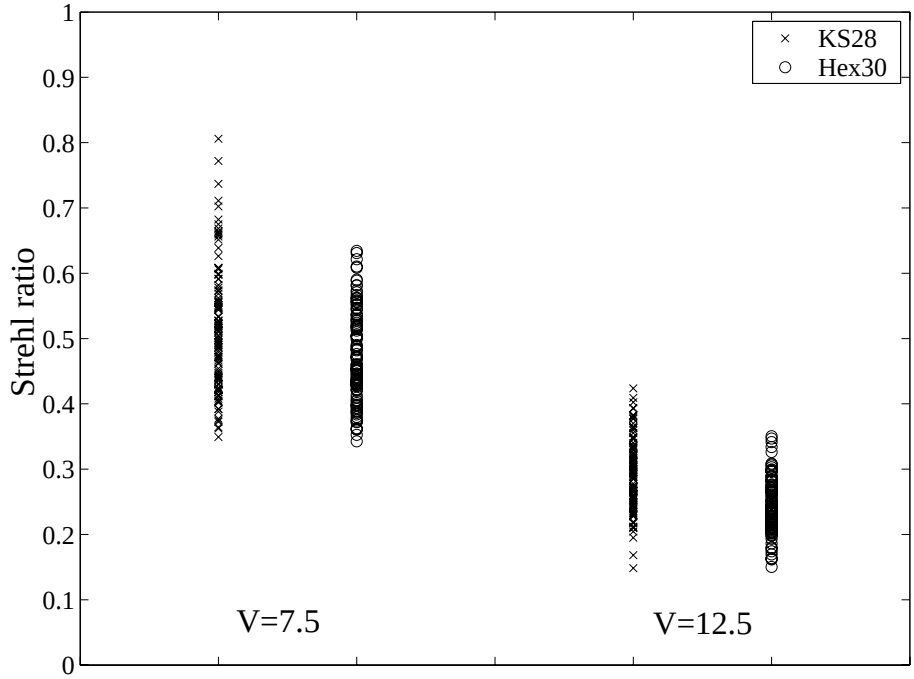

Figure 5. Strehl ratios measured with the KS28 keystone and the HX30 hexagonal array for two guide star brightnesses.

For a statistical analysis of the data, the Kolmogorov-Smirnov test was applied to the samples of 120 Strehl ratio measurements for each configuration. This test showed that these samples do not significantly differ from a normal distribution and a t-analysis on the respective mean values is justified. Table 2 lists the mean Strehl ratios obtained for KS28 and HX30 and different guide star brightness as well as the t-test significance of the hypothesis that both arrays perform equally well. In both cases this hypothesis is rejected with almost certainty, validating the conclusion that the KS28 is superior to the HX30.

Table 2. Results of the lenslet array comparison.

	KS28	HX30	Significance of KS superiority
$m_V = 7.5$	51.5 %	47.4 %	99.99 %
$m_V = 12.5$	29.1 %	24.2 %	99.999 %

4. SUMMARY

Modal wavefront reconstruction with a Shack-Hartmann sensor depends on the geometric interaction between the lenslet array and the modal basis set. Keystone lenslets, up to now only used with Curvature sensors, optimally cover annular telescope pupils and can also be used with the SHS. Current technologies are able to fabricate these arrays similar to hexagonal or rectangular designs and achieve good optical quality.

Model calculations show that the keystone design is superior to the hexagonal one, mainly due to the uniform noise in the lenslets. Care has to be taken that the modal basis set in use interacts well with the lenslet array. While the perfomance of both designs should be similar for high SNR, the keystone design gets the edge for fainter guide stars. The result of the model calculations was confirmed by an experiment, which clearly demonstrated the superiority of the keystone array.

5. REFERENCES

1. Bähr, J., Brenner, *Realization of refractive continuous phase elements with high design freedom by mask structured ion exchange*, Proc. SPIE this issue, 2001
2. Dai, G.-M., *Modal wavefront reconstruction with Zernike polynomials and Karhunen-Loève functions*, JOSA A **13**, 1218-1225, 1996
3. Herrmann, J., *Cross coupling and aliasing in modal wave-front estimation*, JOSA A **71**, 989-992, 1981
4. Kasper, M. E. et al., *ALFA: Adaptive Optics for the Calar Alto Observatory*, Experimental Astronomy **10**, 49-73, 2000
5. Kasper, M. E. et al., *A practical approach to wavefront estimation and modal basis selection*, SPIE Vol. 4007, 592-, 2000
6. Lenzen, R. et al., Omega Cass: a new multimode NIR-imager/spectrometer for the Calar Alto observatory, SPIE Vol. 3354, 493-, 1998
7. Noll, R. J., *Zernike Polynomials and atmospheric turbulence*, JOSA **66**, 207-211, 1976
8. Rigaut, F., Ellerbroek, B. L., Northcott, M. J., *Comparison of curvature -based and Shack-Hartmann-based adaptive optics for the Gemini telescope*, Applied Optics **36**, 2856-, 1997
9. Wang, J. Y., Markey, J. K., *Modal compensation of atmospheric turbulence phase distortion*, JOSA **68**, 78-87, 1978
10. Wizinowich, P. and the Mauna Kea Kamaaina Adaptive Optics Group, *Lessons learned form Adaptive optics on Mauna Kea*, Proc. 'Beyond conventional Adaptive Optics', Venice, 2001